Geomorphology 463 (2024) 109346

Contents lists available at ScienceDirect

Geomorphology

journal homepage: www.journals.elsevier.com/geomorphology

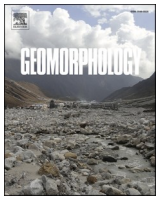

Modelling seasonal variation of sediment connectivity and its interplay with river forms

Linnea Blåfield [a,*], Mikel Calle [a,b], Elina Kasvi [a], Petteri Alho [a]

[a] University of Turku, Department of Geography and Geology, FI-20014, Finland
[b] Department of Geodynamics, Faculty of Geology, Complutense University of Madrid, Madrid, Spain

ARTICLE INFO

Keywords:
Functional sediment connectivity
Close-range remote sensing
Computational fluid dynamics
Fluvial geomorphology

ABSTRACT

Functional connectivity refers to the system dynamics and sediment transfer in a geomorphological system. It is usually quantified through digital elevation models of difference at two time-steps but measuring and quantifying sediment connectivity variation between the time-steps remains a challenge. In this study we utilised a combined approach of morphodynamic model and field observation for assessing seasonal spatio-temporal variation of longitudinal functional connectivity over a 6-kilometre sub-arctic river reach. Comprehensive field datasets including sediment sampling, monitoring of morphological change and continuous discharge and water level measurements, were collected multiple times during the year to calibrate and validate the model for one year. The results revealed that connectivity inside the reach is episodical and not all the morphological adjustment was tied to discharge. Connectivity varied spatio-temporally inside the reach and sediment source and sink areas could be detected. Outside of the hydrological controlled episodes, meander evolutional stage and grain size had notable role in sediment connectivity in the short-term, and therefore underlaying morphological adjustment in the long-term. This approach can contribute to enhancing already existing connectivity indices towards a functional model considering the seasonality and periodicity of connectivity in more detail and would therefore enhance river management and prediction of geomorphic systems functioning.

1. Introduction

The longitudinal transfer of material inside a river reach is usually explained through connectivity – more specifically, functional connectivity, which refers to the flow of water and sediment in a geomorphic system at a certain spatio-temporal scale (Fryirs, 2013; Bracken et al., 2015). It contains understanding the mechanisms, sources and conditions of sediment transport. Dynamic and process-based functional connectivity has received less attention in recent literature compared to structural connectivity, which concentrates on static characteristics of the landscape (Najafi et al., 2021). Those few studies focusing on functional connectivity have quantified it through digital elevation models of difference (DoD) utilizing various connectivity indices (Eltner et al., 2018; Heckmann and Vericat, 2018; James et al., 2019; Calle et al., 2020; Martini et al., 2022). This approach estimates sediment connectivity between two time-steps but lacks the temporal variation between them, as a channel can be connected throughout the year, shorter periods, or during specific hydrological events (Cossart et al., 2018; Keesstra et al., 2018; Poeppl et al., 2020).

In addition to hydrological control, previous studies have shown that physical characteristics of river forms such as meandering or particle size can influence connectivity (Fryirs, 2013; Heckmann et al., 2018; Najafi et al., 2021; Hooke, 2023c). Yet, there are conflicting opinions on whether connectivity should be considered as the cause of the river forms or as the consequence (Fryirs, 2013; Bracken et al., 2015; Wohl, 2017). Nevertheless, connectivity is a crucial component of river morphology and an important driver of system dynamics (Peters and Havstad, 2006). Therefore, it is necessary to understand how it varies between seasons and over time because heterogeneities of connectivity can have drastic impacts on system functioning i.e. sediment transport and morphodynamics. In addition, the need to be able to predict geomorphic systems functioning for future or for decision making requires more detailed understanding of the temporal variation of connectivity.

One solution for assessing the temporal variation of connectivity and its interplay with river forms is computational fluid dynamics (CFD), which is a quantitative modelling tool for complex fluid-flow phenomena based on conservation laws of mass, momentum and energy. Rather

* Corresponding author at: University of Turku, FI-20014, Finland.
E-mail address: linnea.m.blafield@utu.fi (L. Blåfield).

https://doi.org/10.1016/j.geomorph.2024.109346
Received 7 May 2024; Received in revised form 14 July 2024; Accepted 16 July 2024
Available online 23 July 2024

than a more conventional empirical analysis of before/after event changes, CFD enables modelling at high temporal resolution in addition to high spatial one. In order to replicate the processes of a natural river, a comprehensive set of field measurements is needed preferably from different seasons, discharge events and varying conditions to cover all possible situations as it improves the model calibration and validation (Lammers and Bledsoe, 2018; Tangi et al., 2019). However, CFD-models comprising long time periods of sediment connectivity in high spatio-temporal resolution, combined with field measurements are still scarce in the literature, especially at high latitudes (Heckmann et al., 2018; Najafi et al., 2021).

Thus, in this study, we assessed the temporal variation of longitudinal sediment connectivity and its interplay with river forms from a functional perspective in a sub-arctic river by combining morphodynamic CFD-model and field measurements. The aim was to (i) identify possible patterns and seasonal variation of connectivity, (ii) define certain threshold discharges for certain levels of connectivity, and (iii) identify those physical characteristics controlling connectivity at the bend-to-bend scale. CFD was used for modelling the temporal variation of connectivity over one hydrological year, consolidated with comprehensive field measurements for calibrating and validating the model and for quantifying the bend characteristics. This combined approach enabled us to determine the timescale and number of events causing morphological adjustment, and to evaluate whether the physical characteristics of river bends control connectivity or vice versa. This insight provides crucial information of high latitude river's sediment cascade, evolution and morphological functioning.

2. Study area

The sub-arctic Pulmankijoki River, a tributary of the Tana River, is divided into two parts by Lake Pulmankijärvi: the upper course (ca. 50 km) located in Finland and the lower course (ca. 10 km) in Norway—-where it discharges into the Tana River and finally to the Arctic Ocean (Fig. 1A). The river valley is infilled with assorted materials, deposited and reworked over time by glaciofluvial processes, sea phases, and fluvial activity (Mansikkaniemi, 1967; Marthinussen, 1960, 1962). The stratum of these deposits now lies at an altitude of 45–50 m in the valley, and the river has eroded its channel to a depth of 30 m in these bottom deposits. The river has ice-cover from October to May, and the seasonal discharge ranges from 1 to 80 $m^3/s/s$. There are no other flood peaks comparable to the spring flood (Fig. 1C).

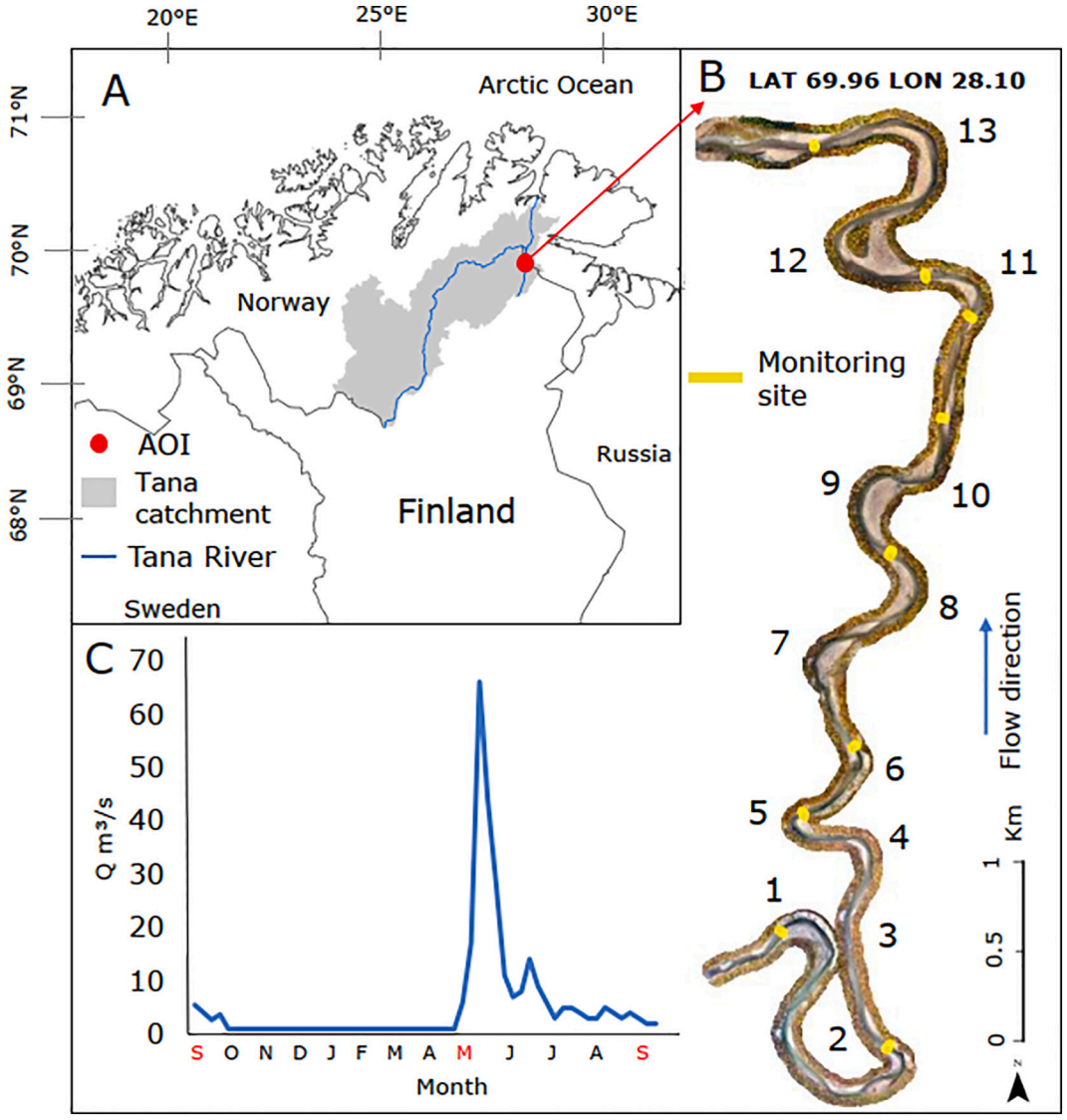

Fig. 1. Map of area of interest (AOI). A) Pulmankijoki River location in Northern Finland. B) The studied reach of Pulmankijoki River and location of discharge and water level monitoring sites. Bends are numbered from upstream (1) to downstream (13). C) Hydrograph of the modelled time period, field work timing is highlighted in red.

The area of interest is a 6-kilometre long reach discharging into the Lake Pulmankijärvi. This reach consists of 13 meander bends with a reach sinuosity of 2.4 (Fig. 1B). The meander bends are of different planform types varying from compound asymmetric bends to simple asymmetric bends. The migration of these bends (6–13) is relatively slow (~0.1 m^{yr}) and most of the morphological changes occur in vertical and longitudinal directions (Kasvi et al., 2013; Lotsari et al., 2014a,b). The mean slope of the study reach is 0.21 m/km, and a sandy bed load dominates the sediment transport. Water of the river is clear (total suspended solids 0 mg/L), except during spring flood, when the amount of suspended material rises to 180–280 mg/L, lasting up to a week.

3. Data, methods, and data processing

Three series of field measurements were carried out during one hydrological year (two in Autumn, A1 and A2, and one in Spring, S1) to collect calibration and validation data for the model. These field campaigns included monitoring of discharge, water level, and sediment, and mapping of the dry and wet geometry. More details in Appendix 1.

3.1. Monitoring of discharge and water level

A total of nine pressure sensors (Solinst, Levelogger 5) were placed in the river channel across the AOI from May to October with approximately 600-meter longitudinal intervals (Fig. 1B monitoring sites). Thus, the sensors spatially cover the whole reach for discharge and water level rating during the open water season with a measurement interval of 15 min. An Acoustic Doppler Current Profiler (ADCP; SonTek/YSI RiverSurveyor M9) was used to measure discharge (Q) from the Levelogger locations (Fig. 1B) daily during the three field campaigns. Similarly, water level (WL) was measured daily from the Levelogger locations (Fig. 1B) with a VRS-GNSS (Virtual Reference Station – Global Navigation Satellite System). Water pressure data was later compensated with an air pressure sensor (Solinst, Barologger) from the same time period and then converted into a continuous hydrograph using the Q and WL measurements and polynomial function. This hydrograph was used as the model input discharge at the upstream boundary. The correlation of water pressure and Q was 0.93 and corresponding value for water pressure and WL was 0.99.

3.2. Mapping geometry and bend characteristics

To create Digital Elevation Models (DEM) and orthomosaics of the study area, two sets of aerial photographs were collected (A1, A2) with a drone DJI Phantom 4. The Phantom 4 has a 12-megapixel camera with a 94-degree field of view aspherical lens which has focal length of 20 mm. For georeferencing the photographs, ground control points (GCP) were installed evenly around the survey area (40 and 41 GCPs in campaigns 1 and 2 respectively). The precise centre point of each GCP was measured with VRS–GNSS. The flight heights above the ground were 50 m, 70 m, and 90 m, as multiple flight altitudes diminish the probability of doming and other systematic errors (Carbonneau and Dietrich, 2017). The camera-viewing angle from 50 m was 30 degrees off-nadir and at nadir from 70 m and 90 m. Photographs were taken with a time-lapse of 2 s. Two flight lines, back and forth, were flown from each altitude along the riverbanks covering the entire channel area with enough picture overlap (Table 1).

Orthomosaics and DEMs were generated from the photographs using commercially available Pix4D-software specifically designed for Structure-from-Motion (SfM) photogrammetry. The image processing methodology is detailed in Micheletti et al. (2015). For further technical details and quality information regarding mosaics, DEMs, image calibration, bundle adjustment, and georeferencing see Table 1.

Later, the DEMs underwent multicamera refraction correction for wet pixels based on Dietrich's work (2017) to diminish the elevation bias caused by the refraction of light through water. Additionally, any elevation errors caused by strong shadows were removed and possible blank areas were interpolated in ArcGIS Pro (v3.0.3). The accuracy of the DEMs was validated against ADCP and VRS-GNSS measurements from the corresponding field campaigns (Table 2). The DEM observed in A1 (DEM-A1) was used as the initial modelling geometry, whereas DEM observed in A2 (DEM-A2) was used for model validation. Meander bend characteristics such as planform type, slope, radius, sinuosity, point bar area and bank height were mapped from the mosaic of A1 based on Hooke (1984), and Frothingham and Rhoads (2003) classification approach.

Table 1
Summary of the observed DEM and orthomosaic quality. A = Autumn.

Feature	DEM-A1	DEM-A2
Average GSD (m)	0.0349	0.0298
Median key points per image	38,248	37,811
Total n. of images	3253	4758
n. of overlapping images	5+	5+
Images calibrated (%)	99	98
Number of GCPs	40	41
RMSE (pixels)	0.174	0.212
Relative difference between initial and optimized camera parameters (%)	2.42	2.36
RMSE GCPs (m)	0.039	0.009

3.3. Sediment and bedload sampling

To monitor changes in grain size, 119 sediment samples (ca. 500 g) were collected from point bar and bank surfaces in A1 and A2. On average 6 samples per meander bend were collected. The samples were dry-sieved using a half-phi interval, and the amount of sediment in each sieve was weighed. D10, D50, and D90 values were calculated for each sample using the method of moments in the GRADISTAT- programme developed by Blott and Pye (2001); it calculates sample statistics logarithmically based on the distribution of phi size values. GRADISTAT classifies samples into textural groups based on sample grain size distribution. It applies its own size scale which differs from other commonly used size scales [e.g. Udden, 1914; Wentworth, 1922; Friedman and Sanders, 1978] by having only four classes (silt, 0.002–0.063 mm; sand, 0.063–2 mm; gravel, 2–64 mm; and boulders, 64–2048 mm). In addition to grain size, a physical description of the sample texture is provided according to Folk (1954).

Furthermore, 12 Helley–Smith bedload transport samples were collected in each campaign from bend 11. Bend 11 was chosen for bedload sampling because a time-series of bedload samples during different seasons has been collected from this bend since 2016 (Lotsari et al., 2019, 2022). Sampling time per sample was 6 min and the sampler was held perpendicular to the flow from a boat. Discharge conditions during sample collection were 7.5 m^3/s, 56 m^3/s, and 4.2 m^3/s in A1, S1, and A2 respectively. These samples were processed and analysed as described above and used for calibrating and validating the modelled bedload.

Table 2
The DEMs were validated against ADCP (wet pixels) and VRS-GNSS (dry pixels) measurements. Correlation (r), R-squared (R^2), mean error (ME), mean absolute error (MAE), and standard deviation of error (SDE) were calculated for each dataset.

DEM validation	r	R^2	ME	MAE	SDE	n
DEM-A1 wet/ADCP A1	0.947	0.905	−0.041	0.13	0.164	384
DEM-A1 dry/VRS-GNSS A1	0.967	0.936	−0.06	0.085	0.106	101
DEM-A2 wet/ADCP A2	0.953	0.91	−0.061	0.08	0.118	259
DEM-A2 dry/VRS-GNSS A2	0.955	0.942	−0.009	0.09	0.104	92

3.4. Physics-based morphodynamic modelling

Morphodynamic modelling (Delft-3D, based on Navier–Stokes' shallow water equations) was used to model the annual water and sediment discharge cycle from September (A1) to September (A2) to determine the temporal variation of the sediment cascade over one hydrological year. Modelling was conducted using a two-dimensional hydrodynamic flow module including morphology. To determine the most suitable simulation parameters, we utilised the sensitivity analysis results similar to those described in Kasvi et al. (2014), Williams et al. (2013) and Williams et al. (2016). The van Rijn (1993) approach was used to solve the sediment input, transport and morphodynamics. A default scheme for dry cell erosion of banks was used which assigns erosion evenly to the adjacent wet and dry cell. No further adjustment of the bank erosion equation was made since the focus was on longitudinal sediment transport. Steady water level and steady discharge (0.63 m^3/s/) were used for the entire ice-covered season based on Lotsari et al. (2020) under ice measurements since Delft-3D cannot implement ice-covered flow. The hydro- and morphodynamic equations in detail can be found, for example, in Kasvi et al. (2014).

The model had a curvilinear grid with an average cell size of 2 × 2 m and hourly varying flow conditions. A spin-up interval of 2880 min was used to reduce noise created by the model. Spatially varying Manning's roughness value based on the sediment sample D50 values was used. Initial conditions were set to match the geometry, water level, and discharge measured in A1. Several calibration simulations with a duration of one month were run over the whole 6-kilometre reach to refine the parametrization using A1 and S1 field data. Once the calibration was successful for both flow scenarios (Fig. 2), the simulation of one year was run. Other modelling parameters are shown in Table 3.

Table 3
Parameters used in the morphodynamic model.

Feature	Parameter
Simulation time	395 days
Output interval (min)	10,080
Number of layers	1
Time step (min)	0.05
Initial geometry	DEM-A1
Spatial buffer up & downstream (m)	200
Upstream boundary	Discharge
Downstream boundary	Water level
Discharge (m^3/s)	Hourly varying
Water level (m)	Hourly varying
Manning's roughness	Spatially varying
Sediment transport formula	van Rijn (1993)
Sediment grain size	Spatially varying (D50 of A1)
Van Rijn reference height	1
Transverse bed slope effect	1.5 (medium)
Min. depth for sed. calculation (m)	0.10
Spin-up interval (min)	2880
Sediment density (kg/m^3)	2650
Water density (kg/m^3)	1000
Gravity (m/s^2)	9.81
Horizontal eddy viscosity (m^2/s)	1

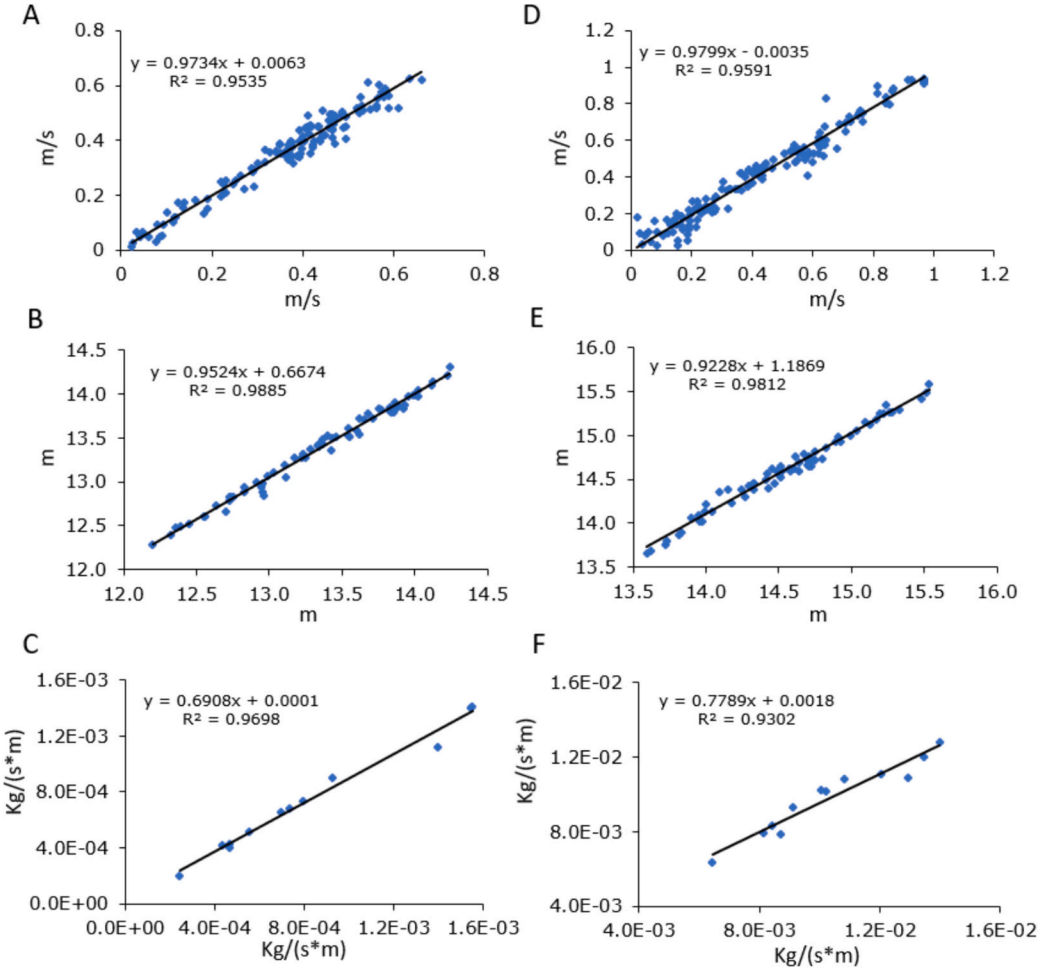

Fig. 2. Model calibration with field data. A) A1 modelled vs. ADCP measured flow velocity. B) A1 modelled vs. VRS-GNSS measured water level. C) A1 modelled vs. measured bedload. D) S1 modelled vs. ADCP measured flow velocity. E) S1 modelled vs. VRS-GNSS measured water level. F) S1 modelled vs. measured bedload.

3.5. Sediment connectivity analysis

Longitudinal functional connectivity was derived from the morphodynamic model results in three extents; 1) Monthly outputs of the model geometry were analysed to obtain the temporal variation of connectivity during the year at reach scale. 2) Sediment budgeting of the morphologically most active period was calculated for quantifying source and sink areas, and sediment transfer from bend-to-bend. 3) Total annual connectivity and net volumetric change were analysed at bend-to-bend scale and their relation to bend characteristics was evaluated.

First, to determine functional Connectivity value (C_v) for each cell of the monthly model outputs, the ratio between total deposited and total eroded sediments per cell was calculated as follows (see Calle et al., 2020):

$$C_v = \frac{Erosion}{Deposition} \quad (1)$$

The outcome of this equation indicates strong connectivity in cells dominated by erosion i.e., cells from which sediment is transported forward ($C_v > 1$) and weak connectivity in cells in which deposition increases in relation to erosion i.e., cells which storages sediment instead of transporting it forward ($C_v < 1$). A C_v of 1 indicates balance between the input and output volumes of the cell i.e., net volumetric change is close to 0. These metrics quantify the functional connectivity towards downstream by indicating high connectivity when sediment is transported forward. However, a cell which is receiving sediment as deposition can be highly connected to upstream. Simultaneously, high connectivity doesn't mean that there's no deposition and vice versa, low connectivity doesn't mean that there's no erosion or sediment transport. Instead, it indicates which of the geomorphic processes is dominant. Likewise, in a balanced situation, there can be sediment transport or even a flush through effect, but the input and output volumes of the cell are closely matched and no significant volumetric surface change occurs.

Secondly, for quantifying sediment transfer between the bends, sediment budgeting from bend-to-bend was calculated as follows:

$$F_i = F_{i-1} + \frac{Erosion_i}{Deposition_i} \quad (2)$$

where F_0 is the initial sediment flux entering the first bend, $Erosion_i$ is the total erosion volume at bend *i*, $Deposition_i$ is the total deposition volume at bend *i*, F_{i-1} is the total sediment flux entering bend *i*, and F_i is the total sediment flux exiting bend *i*.

The outcome of this equation indicates sediment flux volume entering and exiting each bend based on functional C_v. This way, the relative change of sediment flux between bends could be estimated i.e. percentual increase or decrease of flux per bend. The relative change was then combined with total C_v of each bend in order to estimate sediment source and sink areas and the sediment flux behaviour in detail. Lastly, the annual total Cv of the whole reach was calculated based on the net morphological change between the model's first and last time step using Eq. (1).

4. Results

4.1. Model performance

Model calibration and validation indicated that the model performed generally well. Analysis of modelled flow characteristics showed that the water level and velocity were relatively accurate during the entire simulation time, nevertheless showing an increase in error as the model progressed (Table 4). The mean error (ME) of water level increased from 0.03 m in A1 to 0.07 m in S1 and to 0.05 m at the end in A2, representing a 2 %, 7 % and 4 % error respectively. Modelled velocity produced ME of −0.04 m/s in A1, +0.10 m/s in S1 m, and −0.05 in A2, representing errors of −5 %, +14 % and −7 % respectively, indicating that flow velocity for particle motion throughout the model was appropriate.

Table 4
Model validation using field observations. ADCP was used for flow velocity and wet geometry validation, VRS-GNSS for water level and dry geometry validation, Helley-Smith bed load samples for model bed load validation, and refraction corrected DEM-A2 for validating random geometry pixels.

Parameter	r	r2	ME	MAE	SDE	n
Water level (m)						
A1	0.960	0.973	0.031	0.082	0.06	9
S1	0.871	0.915	0.073	0.154	0.147	9
A2	0.917	0.897	0.052	0.103	0.084	9
Flow velocity (m)						
A1	0.914	0.941	−0.042	0.093	0.045	9
S1	0.703	0.731	0.103	0.238	0.231	9
A2	0.849	0.803	−0.054	0.073	0.121	9
Bed load (kg/day * m)						
A1	0.98	0.96	−6	6,7	−3.2	12
S1	0.83	0.80	−31	33	−25	12
A2	0.90	0.88	−7,2	8,5	−4,8	12
Geometry (m)						
ADCP-A2 wet pixel/ DEMmod	0.910	0.855	−0.070	0.262	0.104	259
VRS-GNSS-A2 dry pixel/ DEMmod	0.931	0.897	−0.069	0.085	0.106	91
DEM-A2/DEMmod	0.858	0.777	−0.077	0.239	0.310	422

While the model produced relatively accurate water level and velocity results, the quantity of predicted bed load varied during the simulation time (Table 4). In A1, the modelled and measured bed load had a correlation of 0.98, but during the spring flood the correlation decreased to 0.83, representing ME of −6 kg/day * m (2,8 %) and −31 kg/day * m (8 %) respectively. At the end of the simulation in A2, the correlation of bedload was 0.90, representing ME of −7,2 kg/day * m (3,3 %). The morphological outcome of the model was validated using ADCP, VRS-GNSS and DEM-A2. The model predicted the morphological changes on wet pixels with a correlation of 0.91, and in dry pixels with 0.93 (Table 4). Comparison of random points, both wet and dry, between the DEM-A2 and the modelled DEM (DEMmod) indicated correlation of 0.85 (Table 4).

4.2. Temporal variation of sediment connectivity

Connectivity varied between months based on the model output morphologies (Fig. 3). The whole channel was highly connected ($C_v > 1$) between May and mid-July i.e. during spring flood of >10 m^3/s and moderate flow of >6 m^3/s, indicating sediment being eroded and transported forward or even flushed out of the reach. Spatio-temporal variation of C_v was observed in July, August and September when deposition increased in relation to erosion and all three types of connectivity i.e. high, balanced and low, were observed simultaneously. During this period, the discharge still occasionally exceeded the threshold of 6 m^3/s, but it was not controlling the morphological adjustment anymore. During winter (October to April) there was less variation of monthly C_v. The upstream section was clearly disconnected ($C_v < 1$), whereas rest of the channel was close to balance ($C_v = 1$), indicating that there was sediment transport present but no significant erosion or deposition. It is worth of noting that Fig. 3 does not point out the spatial distribution nor the volume of morphological change (erosion or deposition), but whether the cell is connected to downstream direction or not.

The model indicated that ~70 % of the annual sediment flux took place during spring flood when mean Q was >10 m^3/s, matching the time period of highest C_v (Fig. 4A). In addition, most of the morphological changes (~93 %) took place during this and the following period of moderate flow of Q ~ 6 m^3/s (Fig. 4A–B). The accumulative erosion curve indicated a rapid increase of erosion during the spring flood; likewise the deposition curve showed a rapid increase of deposition

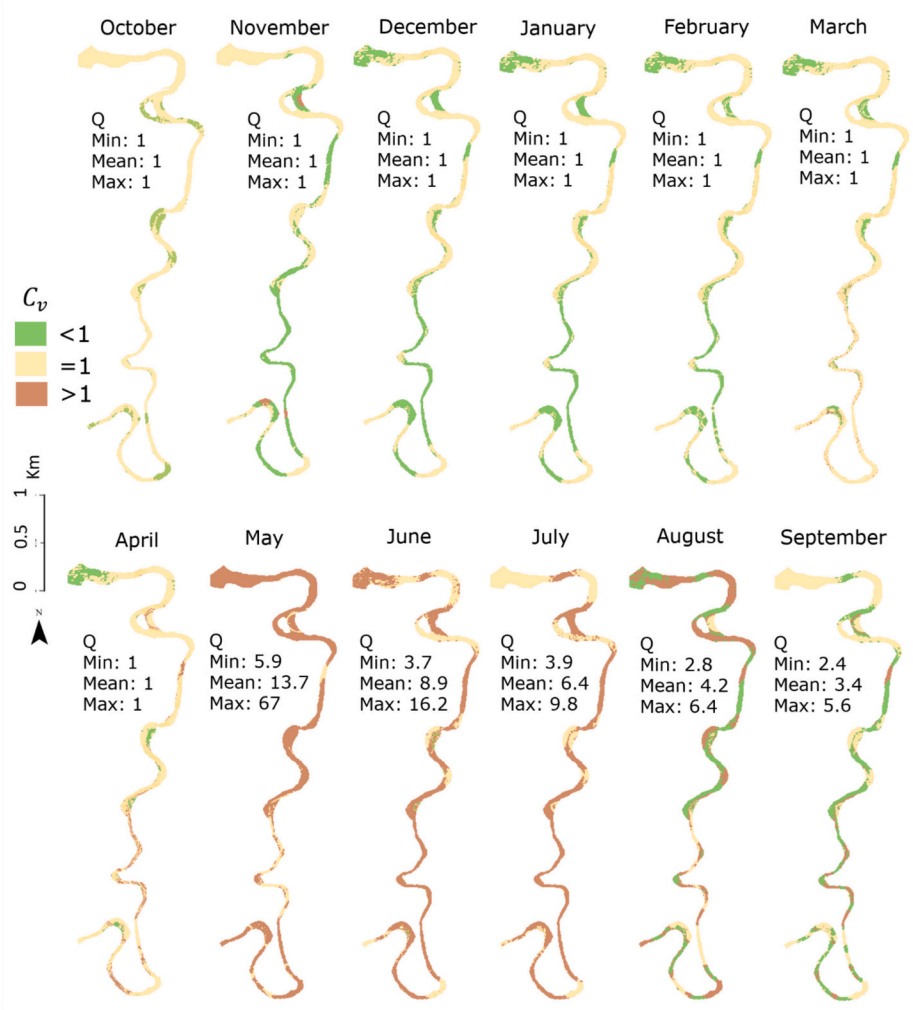

Fig. 3. Monthly variation of functional connectivity (C_v) over the modelled reach. $C_v < 1$ indicates decrease of sediment load being transported downstream. $C_v = 1$ indicates equilibrium; the ratio between sediment entrainment and sediment accumulation is in balance. $C_v > 1$ indicates increase of sediment load being transported downstream. The threshold discharge magnitude (6 m^3/s) for morphological adjustment was exceeded in reach scale during May–July. Spatio-temporal variation of C_v was observed in August and September indicating other controlling factors than discharge.

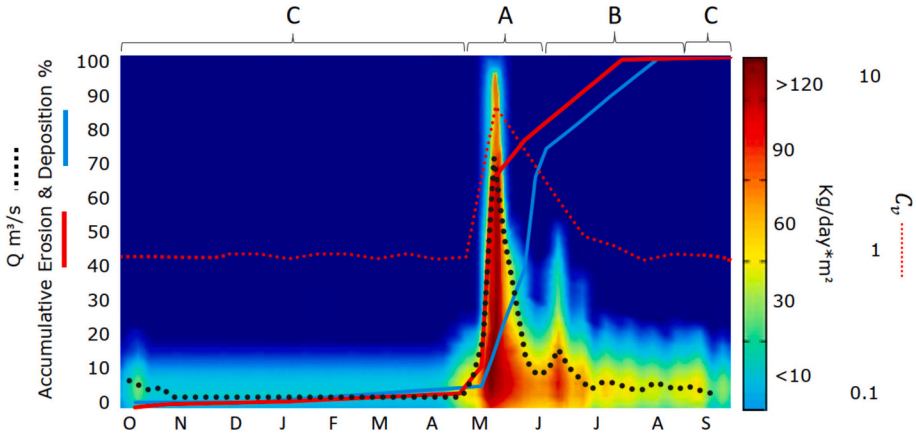

Fig. 4. Modelled total transport volume and its timing during the year plotted with accumulative erosion and deposition curves, annual hydrograph and monthly mean C_v of the reach. A) Highlights the period of high C_v when ~70 % the annual sediment flux and most of the morphological changes occurred. B) Highlights the moderate flow period when C_v and morphological changes started to show spatio-temporal variation and the threshold discharge of 6 m^3/s was still occasionally exceeded. C) No notable changes occurred from September to April, there was very limited amount of sediment transport and channel was either disconnected or balanced.

during the descendent spring flood (Fig. 4). During the moderate flow period (Fig. 4B) the curves were nearly parallel and the C_v decreased. The channel was still mostly mobile, but spatio-temporal variation of connectivity inside the reach was present (Fig. 3). During low flow period ($Q < 3$ m^3/s) the curves are nearly horizontal (Fig. 4C) which supports the observed balanced/disconnected C_v over the same time period, indicating very limited amount of morphological changes (<7 % of total) and sediment transport.

4.3. Bend-to-bend analysis

The model mobilized total amount of 85,011 m^3 of sediment of which 44,227 m^3 (52%) was erosion and 40,784 m^3 (48%) deposition, indicating that 7 % (3443 m^3) of the total mobilized material was transported out of the reach into the Lake Pulmankijärvi. Bend-to-bend budgeting of the modelled sediment flux during the morphologically most active period (A and B episodes as defined in Fig. 4) combined with C_v gives a detailed insight of the sediment cascade and morphological adjustment through the whole river reach. The sediment flux reached its first maximum volume at bend 5, and later 30 % of the flux was deposited on bends 6–8 (1 %, 16 %, and 13 % relative decrease respectively) (Fig. 5). The flux was then reloaded from bends 9–10 (29 % and 17 % relative increase respectively (Fig. 5). At the downstream, 70 % of the remaining sediment flux was deposited on bends 11–13 (1 %, 39 % and 30 % relative decrease respectively) (Fig. 5). After bend 13, the remaining relative 30 % (3443 m^3) of the flux was transported out of the reach, which corresponds to 7 % of the total eroded material.

Generally, the upstream section (bends 1–5) experienced the most erosion, whereas the downstream section gained the most deposition (bends 11–13) (Fig. 6A). Compared to those, the middle reach bends 6–10 experienced more moderate volumetric changes. The annual C_v indicated that the upstream bends 1–5 were highly connected towards the downstream ($C_v > 1$) (Fig. 6B). The middle reach bends (6–10) showed irregular behaviour as all C_v types were present. The downstream bends (11−13) had low connectivity due to heavy deposition. Attention should be paid to what happens in bends 3, 6 and 11, as the relative sediment budgeting and flux curve reveal no or very little change in volume, while the C_v curve indicate balance (Fig. 5). This can be a sign of a flush through effect during the episodes controlled by discharge, or a total change of flux material. These bends experienced similar volumetric changes (nearly 50/50 erosion and deposition), and similar pattern in sediment grain size change (Fig. 6), i.e., coarsening on the upstream and fining on the downstream of the bends. In bends 3 and 6, erosion and deposition areas were divided evenly inside the bend, but in bend 11 the upstream was erosional and downstream depositional based on the surface elevation change (Fig. 6A). This could point to local controlling factors in bend 11.

Sediment samples support the model results. The D50 of all samples increased on average 0.28 mm indicating that also coarse sediment was transported along the reach. However, the magnitude of D50 change was not evenly distributed inside the reach. The largest change up to 1 mm took place at the upstream bends 1 and 2 (Fig. 6C) which also experienced the most erosion. The material eroded from upstream bends was likely transported all the way to bends 6–8 where both, coarse and fine material was deposited (Fig. 6C). The D50 change of middle reach bends was, however, relatively low (0.23 mm increase) which supports the moderate volumetric changes and variation of C_v. Coarse material was likely flushed from bends 9 and 10 when the flux was reloaded causing the D50 to decrease. This slightly coarser material was then deposited at the bends 11 and 12 (Fig. 6C). The finest material was transported all the way to bend 13 or out of the reach. More details of the D50 change in Appendix 1.

The total C_v, total erosion and deposition volumes were compared to the physical meander characteristics observed from the field data (Fig. 7). C_v had highest correlation (−0.47) to planform type indicating high C_v in simple asymmetric (SA) bends and low connectivity in compound asymmetric (CA) bends. A correlation of −0.43 was observed between C_v and bar area, which indicates that large point bars tend to storage sediment leading to low C_v. This is supported by the positive correlation of 0.76 between high deposition proportion (leading to low C_v) and large bar area. In addition, bank height had moderate correlation of 0.42 to C_v, which implies that high banks have the potential to increase downstream connectivity by supplying sediment to the flow. The meander planform type correlation with C_v suggest that young, simple asymmetric bends have higher downstream connectivity than more mature compound bends. This is further supported by the correlation of deposition volume and bar area as compound bends have larger bar area and most of them were located at the downstream section of the reach.

The erosion proportion had the highest correlation to particle D50 change (0.87), indicating that bends which experienced heavy erosion experienced bed coarsening (Fig. 7). Grain size change to finer did not show clear connection to any morphological process, which could indicate that particle settling is more dependent on flow dynamics and transport capacity than local river forms. Bend shape, size and channel length, i.e., sinuosity and radius, indicate correlations of 0.51 and 0.66 to erosion proportion respectively, addressing more erosion in high sinuosity bends with high curvature. For example, bends 1, 2, 4 and 5 experienced heavy erosion (Fig. 6A) and have either high sinuosity, radius or both. Channel slope indicated a correlation of −0.45 and 0.45 to erosion and deposition respectively. This matches with the surface elevation changes in Fig. 6A, since the upstream bends which experienced the most erosion had generally higher slope than the downstream bends. Based on the analysis deposition was more unpredictable and less

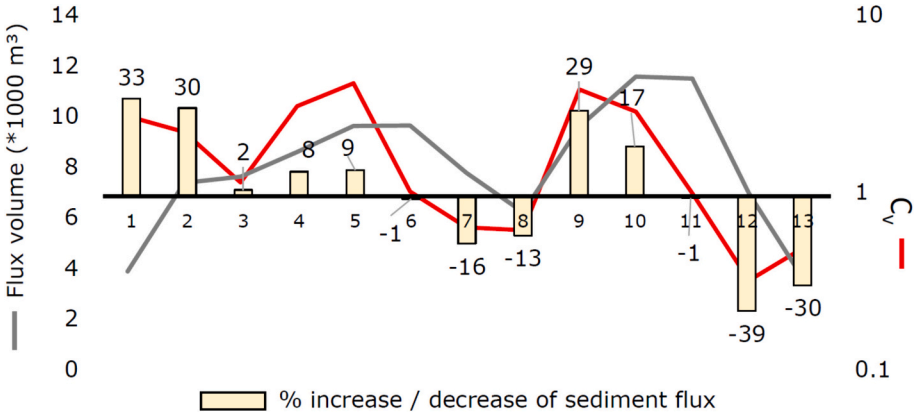

Fig. 5. Budgeting of sediment flux during the morphologically most active period (A + B episodes in Fig. 4) bend-to-bend (1–13) showing the modelled total volume of the flux, Connectivity value (C_v) and relative change of the flux at each bend based on the difference between flux volume when entering and exiting the bend.

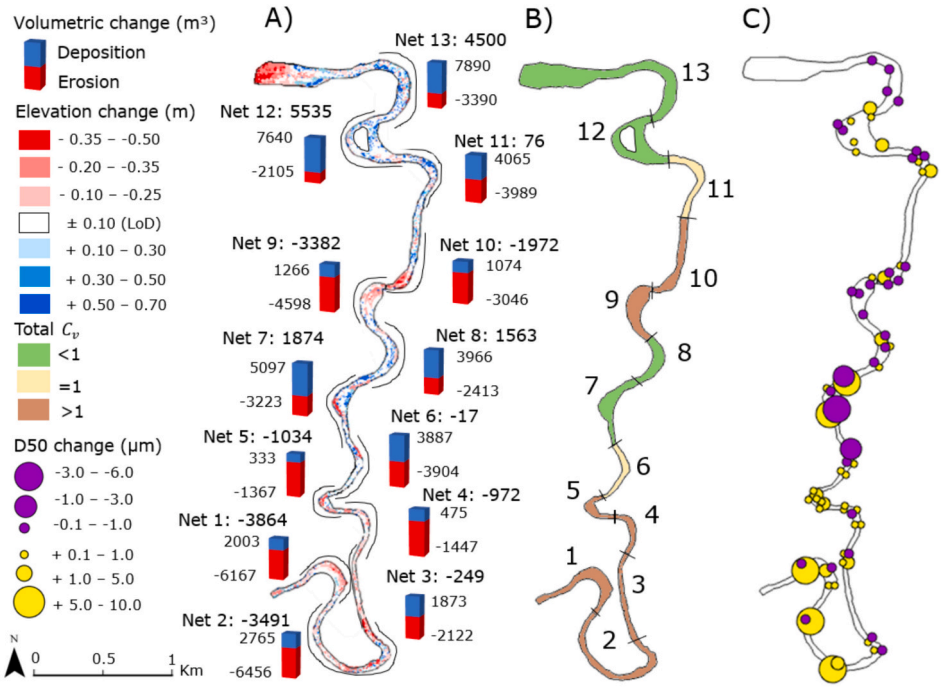

Fig. 6. Bend-to-bend analysis of total change during the modelled year. A) Net volumetric change bend by bend, and surface elevation change of each model cell. B) Bend specific connectivity values based on the net volumetric change over the modelled year. C) Change of particle size D50 value based on the field samples.

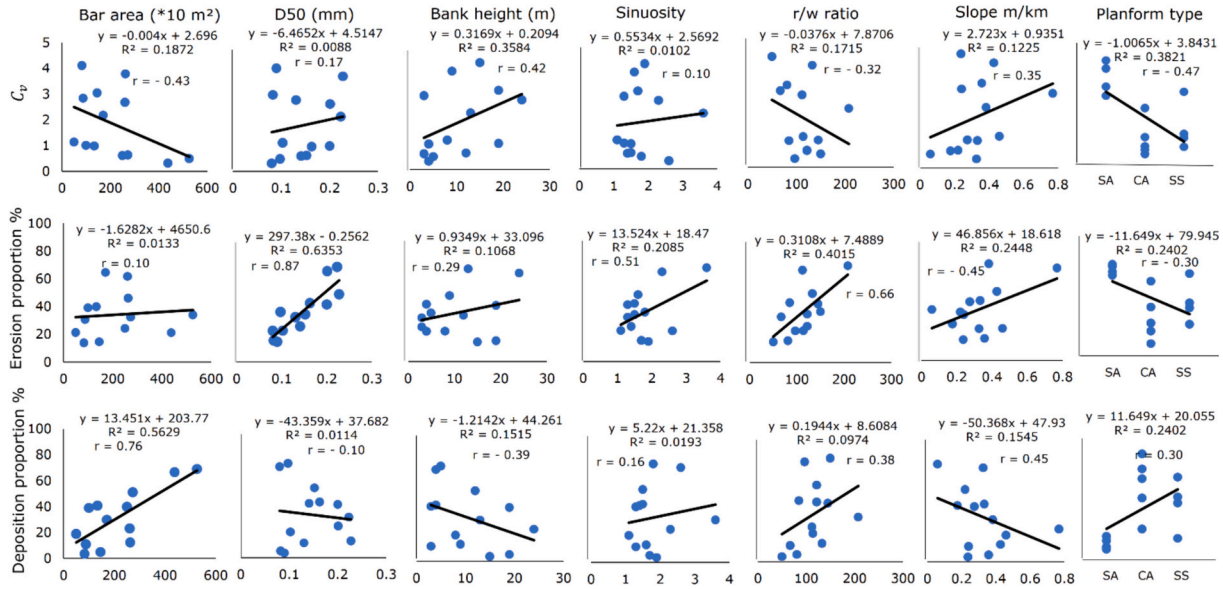

Fig. 7. Meander characteristics measured and mapped from the orthomosaic of A1 plotted with C_v, erosion volume and deposition volume per bend. SA = Simple asymmetric, CA = Compound asymmetric, SS = Simple symmetric.

dependent on river forms than erosion and C_v.

5. Discussion

5.1. Modelling temporal variation of sediment connectivity

The model was able to predict the spatio-temporal variation of functional sediment connectivity during the year with enough reliability. The uncertainty of the model after calibration remained within acceptable limits (excluding peak discharge) according to Pinto et al. (2006) who stated that error of velocity should not exceed 10 % to avoid errors in the predicted sediment flux. Many previous studies using field data as model validation have faced a similar issue of increasing uncertainty during high discharge peaks (Nicholas, 2013; Kasvi et al., 2014; Pajunen et al., 2024). Since the duration of peak discharge was only couple of days, it can be considered that the model worked satisfactorily for the study purpose. The error of bed load during spring flood can be model driven to some extent, but more likely it is related to the field measurement method, as Helley-Smith bed load sampler is known for exaggerative bias (Ryan and Porth, 1999; Vericat et al., 2006). However, the modelled final geometry correlated satisfactorily with the ADCP and VRS-GNSS validation points. The correlations to DEM-A2

were clearly worse, which can be due to field conditions, processing, and corrections needed for creating the DEM itself (Lane et al., 2010; Kasvi et al., 2019).

The model results highlight the temporality of functional connectivity and align with existing knowledge that it is predominantly influenced by discharge (Heckmann et al., 2018; Calle et al., 2020; Zhang et al., 2023). The model indicated high connectivity during the spring flood and moderate flow, while low flow seasons exhibited lower connectivity. Similarly, the most active time period of morphological adjustment was controlled by discharge. Therefore, threshold discharge magnitudes crucial for each connectivity level were determined based on the discharge hydrograph, and the volume of morphological adjustment. This led to categorizing the channel into three distinct temporal episodes utilizing the sediment connectivity framework by Bracken et al. (2015) and coarse sediment transport and (dis)connectivity concepts by Hooke (2003a,b) and Fryirs (2013): 1) Spring flood season ($Q > 10\ m^3/s$) which characterized the high C_v period ($C_v > 1$) lasting for 1,5 months. During this phase, the channel was morphologically most active and experienced erosion, transport, and deposition. 2) Moderate flow period ($Q \sim 6\ m^3/s$) of approximately 2,5 months, when all three classes of C_v were present and both, temporal and spatial variation were observed within the reach. During this episode, erosion decreased relative to deposition and transport. 3) Dormant stage of 7–8 months with C_v around 1 and $Q < 3\ m^3/s$. During this phase minor sediment transport was present without significant erosion or deposition, and the channel was either balanced ($C_v = 1$) or disconnected ($C_v < 1$). Episodes 1 and 2 were responsible of ~90 % of the total sediment flux and morphological change. Worth of noting was that the phenomena behind balanced connectivity in episode 1 and episodes 2–3, can be very different. This indicates that more focus should be paid on the sediment flux properties itself, not solely to surface volume change when evaluating functional connectivity.

The above mentioned episodical behaviour is typical in nival and thermally controlled river systems characterized by a single significant spring flood resulting from snowmelt (Cockburn and Lamoureux, 2008; Shrestha et al., 2021; Buter et al., 2022). Similar conclusions were made by Meybeck et al. (2003) and Syvitski et al. (2022), whom stated that seasonal variation of sediment flux is present in all rivers as most rivers carry their annual load during one season or one flood event. However, changes in sediment flux timing and magnitude are expected globally, and even more in polar and cold regions where hydrological regime is heavily affected by global warming (Syvitski et al., 2022; Zhang et al., 2021). Previous studies have reported increased transport (Syvitski et al., 2005; Zhang et al., 2021; Chalov et al., 2023) and erosion rates (Turcotte et al., 2011; Zhang et al., 2021; Blåfield et al., 2024) due to global warming in cold regions across the world. In addition, reported alteration in high latitude hydrological regime (Arp et al., 2020; Gohari et al., 2022; Blåfield et al., 2024) has the potential alter sediment transport patterns and therefore adjust connectivity. This could lead to several individual episodes of high C_v, mobilizing considerable amounts of sediment, and to increased disconnectivity between them. Hence, we anticipate that more diverse temporal variation of connectivity will occur in the future due to changing hydroclimatic conditions, significantly impacting local morphological adjustment, river system stability, meander evolution and the landscape. Further modelling is needed to evaluate these possible scenarios of future connectivity.

The results of this study highlight the benefits of studying temporal variation of functional connectivity and focusing on the sediment transport process itself, rather than concentrating on static characteristics using only two time-steps over extended period of time. Heterogeneities in sediment transport processes' spatio-temporal dimensions can have drastic impacts on system behaviour i.e. connectivity and morphodynamics. Similar outcomes have been observed by Wainwright (2006) and Turnbull et al. (2008) whom found that heterogeneities can lead to system instability. The approach of combining field measurement and morphodynamic modelling for assessing seasonal variation of connectivity and the interplay with river forms is still rare, but this study demonstrates that it is much needed. This approach can be utilised for enhancing already existing connectivity indices towards a functional model which would consider the seasonality and periodicity of connectivity in more detail, as suggested by Heckmann et al. (2018). That said, longer time-series of functional connectivity modelling is needed for understanding its spatio-temporal scales of sediment transport processes, and to minimize the effect of anomalies and external forcing on functional connectivity. This would enhance the prediction of geomorphic systems functioning in future and assist in decision making, water engineering and river management.

5.2. Sediment connectivity and meander characteristics

Meander characteristics significantly influence sediment connectivity during moderate and low discharge episodes ($C_v = 1$ or $C_v < 1$). During these episodes, the meander bend characteristics drive morphological adjustment, not discharge. Analysis of bend-to-bend morphodynamics revealed in detail the temporal and heterogeneous nature of sediment flux volume, morphological adjustment and sediment connectivity. This is something that traditional sediment budgeting methods are lacking in addition to comprehensive field data (Walling and Collins, 2008; Schwarz et al., 2024). The feedback of sediment flux and process variation was recognised in the morphological adjustment as it resulted in different levels of adjustment between the bends: Upstream bends experienced high erosion rates, downstream bends received more sediment as deposition, and middle reach bends exhibited irregularity with less morphological changes observed. This type of zoning phenomenon influenced by meander characteristics has been previously described by Schumm (1979), Lane (1996), and Hooke (2023c), highlighting the localized feedback and chaotic nature of sediment cascades through the channel.

This perception is supported by the correlation analyses between meander characteristics, C_v, erosion, and deposition volume, as it revealed no significant relationships which highlights the system complexity. The only exception was particle D50 change, which strongly correlated with erosion volume, emphasizing the significant role of particle size in morphological adjustment, also noted by previous studies (Hooke, 2003a,b; Kasvi et al., 2013; Heckmann et al., 2018). Change to coarser material was associated with high erosion rates, while change to finer material was linked with deposition. However, since sand particles are hardly traceable, we cannot validate single particle transport distances. Furthermore, a moderate correlation between C_v and meander planform type suggested that simple asymmetric bends had high downstream connectivity as they experienced significant erosion, while compound bends exhibited lower connectivity to downstream and received sediment as deposition. The moderate correlation between erosion volume and radius, sinuosity, and slope further supports this understanding as they align with the meander bend evolution theories, where young, simple symmetric bends experience more erosion and develop greater radius and sinuosity over time, eventually forming compound bends and cut-offs (Hickin and Nanson, 1984; Hooke, 1984; Frothingham and Rhoads, 2003).

Thus, particle size and the stage of meander development influence connectivity in the short term and their effect is emphasized outside the spring flood season. This conclusion aligns with Peakall et al. (2007), Hooke and Yorke (2010) and Kasvi et al. (2015), whom stated that morphological adjustment dependents on the stage of meander bend development rather than discharge events alone. However, analysis of longer time-series with a boarder set of parameters could yield different conclusions due to complex interactions of erosion, deposition, and meander characteristics. For instance, Lotsari et al. (2014a,b) and Salmela et al. (2020) found significant year-to-year variability between bends inside the same reach despite the consistency in seasonal patterns of morphological adjustment. They found especially deposition areas inconsistent between years, whereas the location of erosion was more

consistent. Likewise, Hooke and Yorke (2010) stated that deposition is more unpredictable than erosion and thus, plays a key role in the morphological feedback of meanders.

Only geomorphological characteristics were analysed in this study, leaving out set of variables which might affect sediment connectivity e.g. flood plain, catchment area and hydrological characteristics. For example, riparian vegetation controls bank erosion and significantly increases deposition on point bars and flood plains (Gorrick and Rodríguez, 2012; Västilä and Järvelä, 2018), which can be one reason for the unpredictability of deposition. Nonetheless, the focus of this study was in functional connectivity i.e. the sediment transport process rather than reach or catchment connectivity, and therefore we only focused on geomorphological parameters of the meanders. We recommend future studies to utilize the combined approach implemented in this study for addressing long-term C_v and morphological adjustment with diverse parametrization.

6. Conclusions

This study examined the seasonal variation of longitudinal sediment connectivity and its interplay with river forms from a functional perspective. Comprehensive field measurements were combined with morphodynamic model spanning over one hydrological year. This approach allowed detailed analysis of functionality of sediment transport, its temporal variation, and assessment of causal connections between river forms and sediment connectivity.

Three different connectivity episodes typical for the river system were detected from the model results. Threshold discharge magnitudes for each episode were defined based on discharge and sediment flux volume. Morphological adjustment during these episodes varied in both temporal and spatial dimensions. Hence, morphological adjustment was not spatio-temporally linear from bend-to-bend during the year. The first two episodes correspond 90 % of the changes recorded indicating that morphological adjustment was controlled by hydrology whenever the threshold discharge magnitude was exceeded. However, during moderate and low flow episodes the role of meander characteristics in sediment connectivity was highlighted. Meander planform type and particle size were found to impact connectivity in short-term which lead to spatial variation of C_v between bends. Thus, bends with similar characteristics tended to behave similarly, reflecting the evolutionary stage of the meander.

These findings support the previous statements about localized and chaotic nature of morphological adjustment, but more importantly, they highlight the importance of studying morphological forms feedback in sediment transport processes and in the development of individual bends. The results underscore the benefits of frequent temporal analysis of sediment connectivity on a somewhat detailed scale, rather than relying on two time-steps over extended periods and a top-down approach.

The approach presented here can be adjusted further for enhancing existing connectivity indices towards functional model which would consider the seasonality and periodicity of connectivity and sediment processes in more detail. Nonetheless, longer time-series of connectivity modelling is needed for understanding the complex relation of river forms and hierarchy of sediment processes, and to minimize the effect of anomalies and external hydrological forcing. Especially focusing on the connectivity episodes where the sediment transport processes were highlighted as a independed function without hydrological control would be beneficial.

CRediT authorship contribution statement

Linnea Blåfield: Writing – original draft, Validation, Methodology, Investigation, Funding acquisition, Formal analysis, Data curation, Conceptualization. **Mikel Calle:** Writing – review & editing, Methodology, Formal analysis, Conceptualization. **Elina Kasvi:** Writing – review & editing, Supervision, Resources, Project administration, Methodology, Conceptualization. **Petteri Alho:** Writing – review & editing, Supervision, Resources, Project administration, Funding acquisition, Conceptualization.

Declaration of competing interest

The authors declare that they have no known competing financial interests or personal relationships that could have appeared to influence the work reported in this paper.

Data availability

Data will be made available on request.

Acknowledgements

This study was funded by the Research Council of Finland through projects “COMBAT” (314312), “InfraRiver” (296090), and “Hydro-RDI” (337279), Turku University Foundation (080797) and Kone Foundation (202104246). We want to thank the current and past members of Fluvial Research Group who participated to the field work.

Appendix 1. The change of D10, D50, D90 and proportion of textural groups between A1 and A2. Textural group classification is based on GRADISTAT's own classification method after Folk, 1954

Location & timing	Sample D10–90 (mm)			Textural group distribution of samples				
Upstream (bends 1–5)	D10	D50	D90	Sand (%)	Slightly gravelly sand (%)	Gravelly sand (%)	Sandy gravel (%)	Gravel (%)
A1	0.12	0.25	0.50	80.0	12.0	4.0	4.0	0.0
A2	0.21	1.33	6.04	25.0	20.0	15.0	35.0	5.0
Middle reach (bends 6–9)								
A1	0.16	0.83	2.02	62.5	12.5	8.3	16.7	0.0
A2	0.19	1.06	4.34	22.7	18.2	31.8	27.3	0.0
Downstream (bends 10–13)								
A1	0.14	0.29	0.57	75.0	15.6	6.3	3.1	0.0
A2	0.24	0.82	2.87	34.6	34.6	11.5	19.3	0.0
Whole reach								
A1	0.14	0.17	1.10	30.9	54.3	6.2	8.6	0.0
A2	0.21	0.45	4.52	11.8	39.7	17.0	30.0	1.5

References

Arp, C.D., Whitman, M.S., Kemnitz, R., Stuefer, S.L., 2020. Evidence of hydrological intensification and regime change from northern Alaskan watershed runoff. Geophys. Res. Lett. 47 (17), e2020GL089186 https://doi.org/10.1029/2020GL089186.

Blåfield, L., Marttila, H., Kasvi, E., Alho, P., 2024. Temporal shift of hydroclimatic regime and its influence on migration of a high latitude meandering river. J. Hydrol. 633, 130935.

Blott, S.J., Pye, K., 2001. GRADISTAT: A grain size distribution and statistics package for the analysis of unconsolidated sediments. Earth Surf. Process. Landf. 26, 1237–1248. https://doi.org/10.1002/esp.261.

Bracken, L.J., Turnbull, L., Wainwright, J., Bogaart, P., 2015. Sediment connectivity: a framework for understanding sediment transfer at multiple scales: sediment connectivity: sediment transfer at multiple scales. Earth Surf. Process. Landf. 40, 177–188. https://doi.org/10.1002/esp.3635.

Buter, A., Heckmann, T., Filisetti, L., Savi, S., Mao, L., Gems, B., Comiti, F., 2022. Effects of catchment characteristics and hydro-meteorological scenarios on sediment connectivity in glacierised catchments. Geomorphology 402, 108128. https://doi.org/10.1016/j.geomorph.2022.108128.

Calle, M., Calle, J., Alho, P., Benito, G., 2020. Inferring sediment transfers and functional connectivity of rivers from repeat topographic surveys. Earth Surf. Process. Landf. 45 (3), 681–693. https://doi.org/10.1002/esp.4765.

Carbonneau, P.E., Dietrich, J.T., 2017. Cost-effective non-metric photogrammetry from consumer-grades UAS: implications for direct georeferencing of structure from motion photogrammetry. Earth Surf. Process. Landf. 42, 473–486. https://doi.org/10.1002/esp.4012.

Chalov, S., Prokopeva, K., Magritsky, D., Grigoriev, V., Fingert, E., Habel, M., Kasimov, N., 2023. Climate change impacts on streamflow, sediment load and carbon fluxes in the Lena River delta. Ecol. Indic. 157, 111252 https://doi.org/10.1016/j.ecolind.2023.111252.

Cockburn, J.M., Lamoureux, S.F., 2008. Hydroclimate controls over seasonal sediment yield in two adjacent High Arctic watersheds. Hydrol. Process.: Int. J. 22 (12), 2013–2027. https://doi.org/10.1002/hyp.6798.

Cossart, E., Viel, V., Lissak, C., Reulier, R., Fressard, M., Delahaye, D., 2018. How might sediment connectivity change in space and time? Land Degrad. Dev. 29 (8), 2595–2613. https://doi.org/10.1002/ldr.3022.

Eltner, A., Maas, H.G., Faust, D., 2018. Soil micro-topography change detection at hillslopes in fragile Mediterranean landscapes. Geoderma 313, 217–232. https://doi.org/10.1016/j.geoderma.2017.10.034.

Folk, R.L., 1954. The distinction between grain size and mineral composition in sedimentary-rock nomenclature. J. Geol. 62, 344–359.

Friedman, G.M., Sanders, J.E., 1978. Principles of Sedimentology. Wiley, New York.

Frothingham, K.M., Rhoads, B.L., 2003. Three-dimensional flow structure and channel change in an asymmetrical compound meander, Embarras River, Illinois. Earth Surf. Process. Landf. 28, 625–644. https://doi.org/10.1002/esp.471.

Fryirs, K., 2013. (Dis) Connectivity in catchment sediment cascades: a fresh look at the sediment delivery problem. Earth Surf. Process. Landf. 38 (1), 30–46.

Gohari, A., Shahrood, A.J., Ghadimi, S., Alborz, M., Patro, E.R., Klöve, B., Haghighi, A.T., 2022. A century of variations in extreme flow across Finnish rivers. Environ. Res. Lett. 17 (12), 124027 https://doi.org/10.1088/1748-9326/aca554.

Gorrick, S., Rodríguez, J.F., 2012. Sediment dynamics in a sand bed stream with riparian vegetation. Water Resour. Res. 48 (2) https://doi.org/10.1029/2011WR011030.

Heckmann, T., Vericat, D., 2018. Computing spatially distributed sediment delivery ratios: inferring functional sediment connectivity from repeat high-resolution digital elevation models. Earth Surf. Process. Landf. 43 (7), 1547–1554. https://doi.org/10.1002/esp.4334.

Heckmann, T., Cavalli, M., Cerdan, O., Foerster, S., Javaux, M., Lode, E., Brardinoni, F., 2018. Indices of sediment connectivity: opportunities, challenges and limitations. Earth Sci. Rev. 187, 77–108. https://doi.org/10.1016/j.earscirev.2018.08.004.

Hickin, E.J., Nanson, G.C., 1984. Lateral migration rates of river bends. J. Hydraul. Eng. 110 (11), 1557–1567. https://doi.org/10.1061/(ASCE)0733-9429(1984)110:11(1557).

Hooke, J.M., 1984. Changes in river meanders: a review of techniques and results of analyses. Prog. Phys. Geogr. Earth Environ. 8, 473–508. https://doi.org/10.1177/030913338400800401.

Hooke, J.M., 2003a. River meander behavior and instability: a framework for analysis. Trans. Inst. Br. Geogr. 28, 238–253. https://doi.org/10.1111/1475-5661.00089.

Hooke, J.M., 2003b. Coarse sediment connectivity in river channel systems: a conceptual framework and methodology. Geomorphology 56, 79–94. https://doi.org/10.1016/S0169-555X(03)00047-3.

Hooke, J., 2023c. Morphodynamics of active meandering rivers reviewed in a hierarchy of spatial and temporal scales. Geomorphology, 108825. https://doi.org/10.1016/j.geomorph.2023.108825.

Hooke, J.M., Yorke, L., 2010. Rates, distributions and mechanisms of change in meander morphology over decadal timescales, River Dane, UK. Earth Surf. Process. Landf. 35 (13), 1601–1614. https://doi.org/10.1002/esp.2079.

James, L.A., Monohan, C., Ertis, B., 2019. Long-term hydraulic mining sediment budgets: connectivity as a management tool. Sci. Total Environ. 651, 2024–2035. https://doi.org/10.1016/j.scitotenv.2018.09.358.

Kasvi, E., Alho, P., Vaaja, M., Hyyppä, H., Hyyppä, J., 2013. Spatial and temporal distribution of fluvio-morphological processes on a meander point bar during a flood event. Hydrol. Res. 44, 1022–1039. https://doi.org/10.2166/nh.2013.091.

Kasvi, E., Alho, P., Lotsari, E., Wang, Y., Kukko, A., Hyyppä, H., Hyyppä, J., 2014. Two-dimensional and three-dimensional computational models in hydrodynamic and morphodynamic reconstructions of a river bend: sensitivity and functionality. Hydrol. Process. 29, 1604–1629. https://doi.org/10.1002/hyp.10277.

Kasvi, E., Vaaja, M., Kaartinen, H., Kukko, A., Jaakkola, A., Flener, C., Hyyppä, H., Hyyppä, J., Alho, P., 2015. Sub-bend scale flow–sediment interaction of meander bends—a combined approach of field observations, close-range remote sensing and computational modelling. Geomorphology 238, 119–134. https://doi.org/10.1016/j.geomorph.2015.01.039.

Kasvi, E., Salmela, J., Lotsari, E., Kumpula, T., Lane, S.N., 2019. Comparison of remote sensing based approaches for mapping geomorphology of shallow, clear water rivers. Geomorphology 333, 180–197.

Keesstra, S., Nunes, J.P., Saco, P., Parsons, T., Poeppl, R., Masselink, R., Cerdà, A., 2018. The way forward: can connectivity be useful to design better measuring and modelling schemes for water and sediment dynamics? Sci. Total Environ. 644, 1557–1572. https://doi.org/10.1016/j.scitotenv.2018.06.342.

Lammers, R.W., Bledsoe, B.P., 2018. Parsimonious sediment transport equations based on Bagnold's stream power approach. Earth Surf. Process. Landf. 43, 242–258. https://doi.org/10.1002/esp.4237.

Lane, S.N., 1996. Environmental Science for Environmental Management. Geogr. J. 162 (1), 100–101. https://doi.org/10.2307/3060252.

Lane, S.N., Widdison, P.E., Thomas, R.E., Ashworth, P.J., Best, J.L., Lunt, I.A., Simpson, C.J., 2010. Quantification of braided river channel change using archival digital image analysis. Earth Surf. Process. Landf. 35 (8), 971–985. https://doi.org/10.1002/esp.2015.

Lotsari, E., Wainwright, D., Corner, G.D., Alho, P., Käyhkö, J., 2014a. Surveyed and modelled one-year morphodynamics in the braided lower Tana River. Hydrol. Process. 28, 2685–2716.

Lotsari, E., Vaaja, M., Flener, C., Kaartinen, H., Kukko, A., Kasvi, E., Hyyppä, H., Hyyppä, J., Alho, P., 2014b. Annual bank and point bar morphodynamics of a meandering river determined by high-accuracy multitemporal laser scanning and flow data. Water Resour. Res. 50, 5532–5559. https://doi.org/10.1002/2013WR014106.

Lotsari, E., Tarsa, T., Kämäri, M., Alho, P., Kasvi, E., 2019. Spatial variation of flow characteristics in a subarctic meandering river in ice-covered and open-channel conditions: a 2D hydrodynamic modelling approach. Earth Surf. Process. Landf. 44, 1509–1529. https://doi.org/10.1002/esp.4589.

Lotsari, E., Dietze, M., Kämäri, M., Alho, P., Kasvi, E., 2020. Macro-turbulent flow and its impacts on sediment transport ppotential of a sub-Arctic river during ice-covered and open-channel conditions. Water 12, 7. https://doi.org/10.3390/w12071874.

Lotsari, E., Lintunen, K., Kasvi, E., Alho, P., Blåfield, L., 2022. The impacts of near-bed flow characteristics on river bed sediment transport under ice-covered conditions in 2016–2021. J. Hydrol. 615, 128610 https://doi.org/10.1016/j.jhydrol.2022.128610.

Mansikkaniemi, H., 1967. Geomorphological Analysis of Pulmanki-Tana Valley in Lapland. Instituti Geographici Universitatis Turkuensis.

Marthinussen, M., 1960. Coast and fjord area of Finnmark. Geol. Norway 208, 416–429.

Marthinussen, M., 1962. C14-Datings Referring to Shore Lines, Transgressions, and Glacial Substages in Northern Norway. (A Supplement to Papers of 1960 and 1961 by the Author).

Martini, L., Cavalli, M., Picco, L., 2022. Predicting sediment connectivity in a mountain basin: a quantitative analysis of the index of connectivity. Earth Surf. Process. Landf. 47 (6), 1500–1513. https://doi.org/10.1002/esp.5331.

Meybeck, M., Laroche, L., Dürr, H.H., Syvitski, J.P.M., 2003. Global variability of daily total suspended solids and their fluxes in rivers. Glob. Planet. Chang. 39 (1–2), 65–93. https://doi.org/10.1016/S0921-8181(03)00018-3.

Micheletti, N., Chandler, J.H., Lane, S., 2015. Structure From Motion (SFM) Photogrammetry. In: Geomorphological Techniques. British Society for Geomorphology, 2047-0371.

Najafi, S., Dragovich, D., Heckmann, T., Sadeghi, S.H., 2021. Sediment connectivity concepts and approaches. Catena 196, 104880. https://doi.org/10.1016/j.catena.2020.104880.

Nicholas, A.P., 2013. Modelling the continuum of river channel patterns. Earth Surf. Process. Landf. 38, 1187–1196. https://doi.org/10.1002/esp.3431.

Pajunen, V., Lotsari, E., Välimäki, J.M., Wolff, F., Kärkkäinen, M., Blåfield, L., Eltner, A., 2024. The impacts of low flow, ice-cover and ice thickness on sediment load in a sub-arctic river–modelling sediment transport with particle image velocimetry calibration data sets. Earth Surf. Process. Landf. 49 (6), 1954–1968. https://doi.org/10.1002/esp.5809.

Peakall, J., Ashworth, P.J., Best, J.L., 2007. Meander-bend evolution, alluvial architecture, and the role of cohesion in sinuous river channels: a flume study. J. Sediment. Res. 77 (3), 197–212. https://doi.org/10.2110/jsr.2007.017.

Peters, D.P.C., Havstad, K.M., 2006. Nonlinear dynamics in arid and semi-arid systems: interactions among drivers and processes across scales. J. Arid Environ. 65 (2), 196–206. https://doi.org/10.1016/j.jaridenv.2005.05.010.

Pinto, L., Fortunato, A.B., Freire, P., 2006. Sensitivity analysis of non-cohesive sediment transport formulae. Cont. Shelf Res. 26, 1826–1839. https://doi.org/10.1016/j.csr.2006.06.001.

Poeppl, R.E., Fryirs, K.A., Tunnicliffe, J., Brierley, G.J., 2020. Managing sediment (dis) connectivity in fluvial systems. Sci. Total Environ. 736, 139627 https://doi.org/10.1016/j.scitotenv.2020.139627.

Ryan, S.E., Porth, L.S., 1999. A field comparison of three pressure-difference bedload samplers. Geomorphology 30 (4), 307–322. https://doi.org/10.1016/S0169-555X(99)00059-8.

Salmela, J., Kasvi, E., Vaaja, M.-T., Kaartinen, H., Kukko, A., Jaakkola, A., Alho, P., 2020. Morphological changes and riffle-pool dynamics related to flow in a meandering river channel based on a 5-year monitoring period using close-range remote sensing. Geomorphology 352. https://doi.org/10.1016/j.geomorph.2019.106982.

Schumm, S.A., 1979. Geomorphic thresholds: the concept and its applications. Trans. Inst. Br. Geogr. 485–515. https://doi.org/10.2307/622211.
Schwarz, S., Rindler, R., Liedermann, M., Shire-Peterlechner, D., Lammer, A., Tritthart, M., Habersack, H., 2024. Challenges and opportunities of sediment budgeting using the River Sediment Budget Approach (RSBA): three cases in Austrian gravel-bed river reaches. Geomorphology, 109182. https://doi.org/10.1016/j.geomorph.2024.109182.
Shrestha, R.R., Pesklevits, J., Yang, D., Peters, D.L., Dibike, Y.B., 2021. Climatic controls on mean and extreme streamflow changes across the permafrost region of Canada. Water 13 (5), 626. https://doi.org/10.3390/w13050626.
Syvitski, J.P., Kettner, A.J., Correggiari, A., Nelson, B.W., 2005. Distributary channels and their impact on sediment dispersal. Mar. Geol. 222, 75–94. https://doi.org/10.1016/j.margeo.2005.06.030.
Syvitski, J., Ángel, J.R., Saito, Y., Overeem, I., Vörösmarty, C.J., Wang, H., Olago, D., 2022. Earth's sediment cycle during the Anthropocene. Nat. Rev. Earth Environ. 3 (3), 179–196. https://doi.org/10.1038/s43017-021-00253-w.
Tangi, M., Schmitt, R., Bizzi, S., Castelletti, A., 2019. The CASCADE toolbox for analyzing river sediment connectivity and management. Environ. Model Softw. 119, 400–406. https://doi.org/10.1016/j.envsoft.2019.07.008.
Turcotte, M.M., Reznick, D.N., Hare, J.D., 2011. The impact of rapid evolution on population dynamics in the wild: experimental test of eco-evolutionary dynamics. Ecol. Lett. 14 (11), 1084–1092. https://doi.org/10.1111/j.1461-0248.2011.01676.x.
Turnbull, L., Wainwright, J., Brazier, R.E., 2008. A conceptual framework for understanding semi-arid land degradation: ecohydrological interactions across multiple-space and time scales. Ecohydrol.: Ecosyst. Land Water Process Interact. Ecohydrogeomorphol. 1 (1), 23–34. https://doi.org/10.1002/eco.4.
Udden, J.A., 1914. Mechanical composition of clastic sediments. Geol. Soc. Am. Bull. 25, 655–744.
van Rijn, L.C., 1993. Principles of Sediment Transport in Rivers, Estuaries and Coastal Seas. Aqua Publications, The Netherlands. https://doi.org/10.1016/j.geomorph.2014.01.018.
Västilä, K., Järvelä, J., 2018. Characterizing natural riparian vegetation for modeling of flow and suspended sediment transport. J. Soils Sediments 18, 3114–3130. https://doi.org/10.1007/s11368-017-1776-3.
Vericat, D., Church, M., Batalla, R.J., 2006. Bed load bias: Comparison of measurements obtained using two (76 and 152 mm) Helley-Smith samplers in a gravel bed river. Water Resour. Res. 42 (1) https://doi.org/10.1029/2005WR004025.
Wainwright, J., 2006. Degrees of separation: hillslope-channel coupling and the limits of palaeohydrological reconstruction. Catena 66 (1–2), 93–106. https://doi.org/10.1016/j.catena.2005.07.016.
Walling, D.E., Collins, A.L., 2008. The catchment sediment budget as a management tool. Environ. Sci. Pol. 11 (2), 136–143. https://doi.org/10.1016/j.envsci.2007.10.004.
Wentworth, C.K., 1922. A scale of grade and class terms for clastic sediments. J. Geol. 30, 377–392.
Williams, R.D., Brasington, J., Hicks, M., Measures, R., Rennie, C.D., Vericat, D., 2013. Hydraulic validation of two-dimensional simulations of braided river flow with spatially continuous aDcp data. Water Resour. Res. 49 (9), 5183–5205.
Williams, R.D., Measures, R., Hicks, D.M., Brasington, J., 2016. Assessment of a numerical model to reproduce event-scale erosion and deposition distributed in a braided river. Water Resour. Res. 52, 6621–6642. https://doi.org/10.1002/2015WR018491.
Wohl, E., 2017. Connectivity in rivers. Prog. Phys. Geogr. 41 (3), 345–362. https://doi.org/10.1177/0309133317714972.
Zhang, Y., Huang, C., Zhang, W., Chen, J., Wang, L., 2021. The concept, approach, and future research of hydrological connectivity and its assessment at multiscales. Environ. Sci. Pollut. Res. 28, 52724–52743. https://doi.org/10.1007/s11356-021-16148-8.
Zhang, T., Li, D., East, A.E., Kettner, A.J., Best, J., Ni, J., Lu, X., 2023. Shifted sediment-transport regimes by climate change and amplified hydrological variability in cryosphere-fed rivers. Sci. Adv. 9 (45), eadi5019 https://doi.org/10.1126/sciadv.adi5019.

Further reading

Lammers, R.W., Bledsoe, B.P., 2018. A network scale, intermediate complexity model for simulating channel evolution over years to decades. J. Hydrol. 566, 886–900. https://doi.org/10.1016/j.jhydrol.2018.09.036.